EDGE ARTICLE

Army ants tunneling for classical simulations†

Jingjing Zheng, Xuefei Xu, Rubén Meana-Pañeda and Donald G. Truhlar*

The classical trajectory method (also called molecular dynamics) is the most widely used method for ensemble averaging and calculating rate constants of complex dynamical systems; however it has the serious drawback of not allowing tunneling. Here, we show how to include tunneling efficiently in real-time classical trajectories by using the army ants algorithm for quantum mechanical rare event sampling and partially optimized semiclassical tunneling paths based on valence internal coordinates. Three examples, HN_2 dissociation and two kinds of HCOH isomerizations, are used to illustrate the tunneling method. We show that the army ants tunneling algorithm is very efficient (even lower computational costs than calculations without tunneling) and yields physically reasonable rate constants. The new algorithm is straightforward to include in any molecular dynamics package, and it allows sampling of regions of phase space that are classically inaccessible but that may lead to different products or different energy distributions than are populated by non-tunneling processes.

Introduction

The classical trajectory method[1,2] is the most widely used approximation for molecular dynamics simulations of chemical processes. It is very general, and it can be approximately justified because the de Broglie wavelength for nuclear motion is usually small compared to the characteristic length on which the potential energy changes. The classical trajectory method has two well-known major deficiencies though: (1) bound vibrational motions can have any energy with no reference to quantized vibrational energy levels of the quantum mechanical stationary states; (2) tunneling is neglected.

Deficiency no. 1 is most serious for low vibrational energies, and a chief symptom is that systems are not required to have zero point energy (ZPE). (Zero point energy is an exact constraint only for stationary states, but we know from extensive experience with approximate and accurate solutions of the Schrödinger equation that it is an approximate local constraint on bound vibrational modes even during dynamics.) Various approximation schemes have been proposed to alleviate this difficulty, *e.g.*, quantization at the beginning of a trajectory[3] (the so-called quasiclassical trajectory method), enforcing energy transfer between modes during a trajectory,[4,5] or treating bonds with high-frequency vibrations as rigid.[6] None of these procedures is satisfactory for all situations, but nevertheless they can be helpful and have been found useful. But including ZPE in classical trajectories is beyond the scope of the present article.

Department of Chemistry, Chemical Theory Center, and Supercomputing Institute, University of Minnesota, Minneapolis, MN 55455-0431, USA. E-mail: truhlar@umn. edu

Deficiency no. 2 affects not just classical trajectory calculations but also many wave packet methods where the center of the wave packet follows a classical trajectory.[7] In this article, we propose a simple method, called army ants tunneling, to include tunneling in real-time classical trajectory calculations.

A variety of semiclassical methods have been proposed for tunneling calculations, but we will limit our attention here to the ones most related to the present work. Previously, semiclassical methods for calculating tunneling probabilities have been developed successfully for calculating thermal reaction rates in the variational transition state theory framework, where dominant tunneling paths start and end near a minimum energy path.[8] In approximations (called large-curvature tunneling[9,10] and least action tunneling[11,12]) that turned out to have the broadest general validity,[13] tunneling occurs along straight-line (rectilinear) paths (in the limit of large reaction-path curvature) or optimized paths (in the more general case) from a caustic surface of bound vibrational motion in the reactant region to a caustic surface of bound vibrational motion in the product region. (A caustic is a surface that separates the region visited by classical trajectories from regions not visited.) Similar tunneling paths emanating from caustic surfaces were proposed for electronically nonadiabatic processes where the state with the largest tunneling probability will dominate, and this will often be the state with the shortest tunneling path.[14] In general, from a semiclassical perspective, the optimum tunneling path is the one with the least imaginary action,[11,12] which is a compromise between a low-energy path, a short path, and a path with a low reduced mass. In this semiclassical spirit, adding straight-line tunneling paths normal to caustic surfaces was suggested for use in classical trajectory simulations[15] *via* a branching model that was originally proposed[16] for surface hopping.

The addition of tunneling paths to trajectories has been used for calculating isomerization tunneling splittings where the final terminus of the tunneling path is taken as a caustic of the isomerized well and where one calculates an average tunneling amplitude by averaging a trajectory in one well rather than branching.[17–19] Why is tunneling not incorporated in classical simulations more broadly? One reason is that the proposed branching[15] is carried out as for the anteater algorithm[16] originally proposed for surface hopping. In particular, when a system reaches a turning point in some mode, a tunneling probability P_t is computed for a straight tunneling path along the direction of that mode, and the tunneling path is followed if P_t exceeds a random number λ (all random numbers in this article are uniform on $[0, 1]$). If P_t is, for example, 10^{-3} or less, it means that one tunneling path is followed on average for each one thousand or more tunneling events; therefore trajectories will rarely tunnel, and the method will be inefficient for sampling tunneling events. A second reason is that rectilinear tunneling paths (*i.e.*, paths that are straight in Cartesian coordinates) in the direction normal to a caustic surface may be far from optimum and may even lead to negligible tunneling probability. Here we propose improvements motivated by both of these shortcomings.

Prior to the army ants algorithm, two methods were used for sampling trajectories. In one, called the ants algorithm, trajectories would be bifurcated at a quantum event (tunneling in the present context, surface hopping in the original context[16]), and one would follow the quantum branch with weight P_t *and* the non-quantal branch with weight $1 − P_t$; this has the disadvantage of often leading to an impractically large number of branches to follow, where the large number of branches resemble a swarm of ants. The alternative is to follow the quantal branch with probability P_t *or* the non-quantal branch with probability $1 − P_t$ (like an anteater, this scheme follows mainly the paths where ants, *i.e.*, trajectories, are most likely to be found); this has the disadvantage for small P_t that one seldom follows the interesting quantal branches. To make rare-event sampling more efficient we replace the anteater algorithm[16] by the army ants algorithm introduced earlier[20] for rare events in surface hopping.

Furthermore we partially optimize the tunneling paths by using curvilinear coordinates instead of rectilinear coordinates, *i.e.*, using valence internal coordinates. It is known from vibrational spectroscopy and successful molecular mechanics methods that valence internal coordinates (bond stretches, bond angle bends, and torsions) are much less strongly coupled than rectilinear normal modes,[21] and normal-mode motion is only valid for small amplitude motion since normal modes are based on the harmonic-oscillator approximation. In fact, even along reaction coordinates, rectilinear motion is much less physical than valence coordinate motions.[22,23] Thus a simple way to partially optimize tunneling paths for general situations is to replace rectilinear motion by motion along a valence internal coordinate, such as a bond stretch, bond angle bend, or torsion, or by motion along a combination of two or more valence internal coordinates, such as a difference of two stretch coordinates for atom-transfer reactions. Therefore, in the

application presented here, we use motions along internal coordinates as our tunneling paths.

A consequence of the variational principle that the optimized tunneling path is the tunneling path with the least imaginary action is that the optimum tunneling path should have the largest tunneling probability. In practice it is impractical to completely optimize the tunneling path. The specific partial optimization scheme proposed in the paper is only one possibility, but it is sufficient to illustrate the new method for including tunneling. Experience shows that partial optimization of tunneling paths is often very useful, and it has been used successfully in many previous applications of multidimensional tunneling methods with variational transition state theory; this includes reactions in the gas phase, in liquid-phase solution, at gas–solid interfaces, and in enzymes.[8,11–13,24] The present paper allows one to include this kind of tunneling calculation in molecular dynamics simulations.

Methods

In this section we present the details of the army ant branching algorithm for the sampling of rare events and how the tunneling path and action integral are computed in internal coordinates.

Army ants branching algorithm

Each trajectory starts with a weight of unity. When a tunneling probability P_t is calculated for a possible tunneling path, we take two steps to determine if the trajectory is branched or not and how the weight of a trajectory is changed: (1) one computes $\gamma = \max(\eta, P_t)$ where η is a parameter, and picks a random number λ_1. If $\lambda_1 > \gamma$, there is no tunneling, and the classical trajectory continues without changing its weight. (2) If $\lambda_1 < \gamma$, one picks another random number λ_2, and if $\lambda_2 > 0.5$, there is still no tunneling, but the weight of the trajectory is decreased by a factor $1 − P_t/\gamma$. However if $\lambda_2 < 0.5$, one accepts the tunneling path and its weight is changed by a factor of P_t/γ. Consequently we follow tunneling events about half the time when η is chosen to a value close to 1, but they are weighted to ensure that the result converges to the same probability of tunneling as in the anteater method. Since, very often, $P_t \ll 0.5$, the statistics on tunneling events are greatly improved, and we can efficiently explore regions of space reached only by tunneling.

The choice of η affects the rate of convergence with respect to the number of trajectories but not the converged results, so this choice is a practical matter. Calculations in this article were carried out with η taken as 0.95. Some examples of calculations with other values of η are also given for discussion.

Tunneling path

The trajectory is monitored at every integration step to see if it reaches a turning point of the tunneling coordinate, where that coordinate reaches a maximum or minimum, *i.e.*, where $\mathbf{p} \cdot \mathbf{d}_0$ is zero, where $\mathbf{p}$ is the momentum and $\mathbf{d}_0$ is the unit vector along the tunneling direction that defines the initial direction of the tunneling in (unscaled) Cartesian coordinates. In the current study, the tunneling direction is chosen to be a single valence

internal coordinate or a combination of internal coordinates. The unit vector $\mathbf{d}_0$ is calculated as $\Delta\mathbf{x}_0/|\Delta\mathbf{x}_0|$ where $\Delta\mathbf{x}_0$ is a small displacement of Cartesian coordinate along the tunneling direction from the current geometry. The Cartesian displacement can be calculated by

$$\Delta\mathbf{x}_0 = \mathbf{A}\Delta\mathbf{R}_0 \tag{1}$$

where $\mathbf{A}$ is a generalized inverse matrix of the Wilson $\mathbf{B}$ matrix,[25] and $\Delta\mathbf{R}_0$ is a column vector of internal coordinate displacements. Eqn (1) is only accurate to first order, and it is used iteratively until $\Delta\mathbf{x}_0$ is converged.[26] When the tunneling direction is along one single coordinate or a combination of two internal coordinates, all elements of $\Delta\mathbf{R}_0$ are zero except the one or two that correspond to the tunneling direction. More generally each element of $\Delta\mathbf{R}_0$ represents a small displacement of an internal coordinate along the tunneling direction. Atom-transfer reactions involve significant changes of at least two bond lengths; for a bond length displacement of the breaking bond equal to Δr (where $\Delta r > 0$), we set the bond length displacement of the forming bond equal to $-l\Delta r$, where l is an adjustable synchronicity parameter. The optimum tunneling path is the one with the greatest tunneling probability,[11,12] so we can optimize the path by varying l. It is possible to optimize trial tunneling paths with more parameters, but in the present article we restrict ourselves to the simple choices just presented.

When a turning point is reached, we calculate the tunneling probability in the isoinertial coordinate system $\mathbf{q}$ related to the $3N$-dimensional Cartesian coordinate $\mathbf{x}$ by

$$\mathbf{q} = \mathbf{m}^{1/2}\mathbf{x}/\mu^{1/2} \tag{2}$$

where $\mathbf{m}$ is a diagonal matrix of order $3N$ containing three copies of each of the N atomic masses associated with each of the $3N$ unscaled Cartesian coordinates, and μ is any constant reduced mass. Then the tunneling probability is $P_t = e^{-2\theta}$ where θ is the imaginary action integral calculated along the tunneling path and given by

$$\theta = \frac{1}{\hbar}\int_0^{\xi_{max}} \sqrt{2\mu[V(\mathbf{q}) - V(\mathbf{q}_0)]}\mathrm{d}\xi \tag{3}$$

where ξ is the distance along the tunneling path of position $\mathbf{q}$ relative to the starting point of tunneling path $\mathbf{q}_0$, ξ_{max} is the length of whole tunneling path in isoinertial coordinates, and we have used the fact that the isoinertial coordinate system has the same reduced mass μ in all directions of $3N$-dimensional space. The physical reasoning leading to eqn (3) is the same as used previously.[9,15]

Calculations

To illustrate the new method, we made calculations for hydroxycarbene isomerizations and HN_2 radical dissociation in their ground electronic states:

$$cis\text{-HCOH} \rightarrow trans\text{-HCOH} \tag{R1}$$

$$HN_2 \rightarrow H + N_2 \tag{R2}$$

$$trans\text{-HCOH} \rightarrow H_2CO \tag{R3}$$

The potential energy surface for (R1) and (R3) is calculated by the PDDG/PM3 (ref. 27) method, and the trajectories are carried out by direct dynamics by coupling a modified version of the ANT[28] program with the MOPAC-mn[29] program. An analytic potential energy surface[30] is used for the HN_2 dissociation. Reaction (R1) has a barrier of 1.09 eV along the H–C–O–H torsional coordinate, reaction (R2) has a barrier to dissociation of 0.50 eV, and reaction (R3) has a barrier of 1.57 eV to transfer of H; see Fig. 1.

The ensemble of initial states was selected to be random except for the fixed total internal energy E and the total angular momentum fixed at zero. For each energy, NVE ensembles have 10 000 trajectories for R1 and 100 000 trajectories for (R2) and (R3). To obtain better convergence for demonstrating the results with various η values, we also ran 400 000 trajectories for (R2) at energy 0.44 eV. We used a 4th order Runge–Kutta integrator with a step size of 0.1 fs.

In each case, we define a complete set of $3N - 6$ nonredundant internal coordinates, where N is the number of atoms; then we define a tunneling direction. The tunneling direction for (R1) is the torsion angle, for (R2) it is the H–N1 bond length (where N1 is the nitrogen closer to H), and for (R3) it is a combination of decreasing the forming C–H_t bond length and increasing the O–H_t bond length in a ratio $l : 1$, where H_t is the transferred hydrogen atom, and l is a fixed parameter for a given
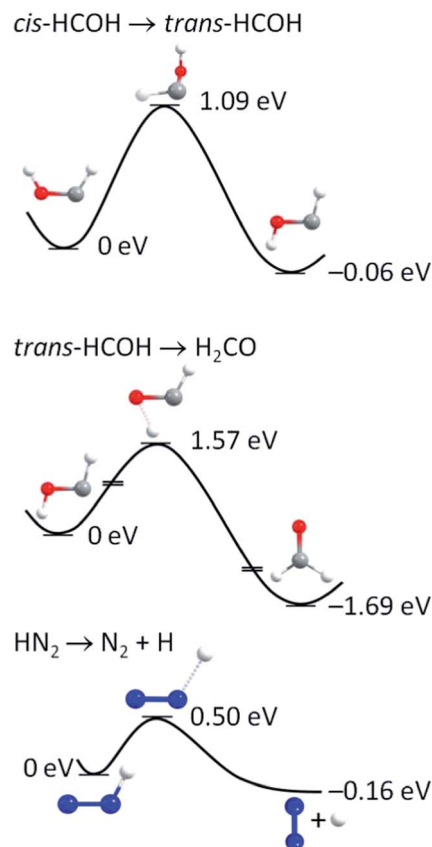

Fig. 1 Potential energy profiles.

calculation on an ensemble of trajectories. Thus for (R1) and (R2), the internal coordinate displacement vectors in eqn (1) have all elements zero along tunneling path except the H–C–O–H dihedral angle and the bond length H–N1 respectively. For (R3), the elements of the internal coordinate displacement vector corresponding to the changes of C–H_t and O–H_t bonds are $-l\Delta r$ and Δr along the tunneling path, and the other four internal coordinate displacements (C–H bond, C–O bond, H–C–O angle, and the bending angle of O out of the C–H–H_t plane) are zero. The value of Δr is zero at the initial turning point and gradually changes to a positive value that gives the same energy as that of the initial turning point. In defining a set of non-redundant internal coordinates for (R3), we took care that any internal coordinate involving H_t that is not fixed along the tunneling path should not be included in the $3N - 8$ internal coordinates that are not involved in the tunneling direction. For example, with our choice of internal coordinates, when H_t is moving along the tunneling path, the C–H_t–O angle is not fixed.

Reaction is assumed to have occurred and the trajectory stopped when the torsion angle is between 130 and 180 deg. or between -180 and -130 deg. (R1), when the H–N1 distance is equal to or larger than 4 Å (R2), or when the new C–H bond is equal to or smaller than 1.2 Å (R3). The reaction probability P_r at time t equals the sum of the weights of trajectories that have already reacted divided by the sum of the weights of all trajectories at this point in time.

To calculate the rate constant $k(E)$, we assume the following relation between number of non-reactive trajectories ($N_{nonreact}$) and the total number of trajectories (N_{total}) at time t for an ensemble with energy E if each trajectory is equally weighted

$$N_{nonreact}(E) = N_{total}(E)\exp(-k(E)t) \qquad (4)$$

If we write the reaction probability as $P_r(t) = (N_{total} - N_{nonreact})/N_{total}$ at time t, then eqn (4) can also be written as

$$\ln(1 - P_r) = -k(E)t \qquad (5)$$

Therefore, reaction rate $k(E)$ can be obtained by fitting the linear (or nearly linear) region of the decay curve of $\ln(1 - P_r)$ vs. t. When each trajectory is weighted by the army ants algorithm, the reaction probability $P_r(t)$ is given as

$$P_r(t) = \frac{\sum_{j=1}^{N_{react}} W_j(t)}{\sum_{i=1}^{N_{total}} W_i(t)} \qquad (6)$$

where N_{react} is the number of reactive trajectories, and $W_i(t)$ is the weight of trajectory i at time t, and $W_j(t)$ is the weight of reactive trajectory j at time t.

Results and discussion

The decay of the logarithm of the nonreactive probability, $\ln(1 - P_r)$, is plotted in Fig. 2 for reactions (R1) and (R2); the negative slopes of each line after the induction period are the steady-state rate constants, which will be given in a later figure. Without including tunneling, both reactions take a much longer time to reach the first order decay rate and have smaller decay rates by about two orders of magnitude. We noticed that the curves with tunneling are not as smooth as those without tunneling and also noticed that decay curves with tunneling have much smaller nonreactive probabilities. The scatter in the decay curves with tunneling occurs in the region where the number of remaining non-reactive trajectories is small leading to inevitable numerical noise in the sampling if the simulation is carried to long enough time. (The scatter on the curves with tunneling does not result from the tunneling method but rather from following the ensemble until there are few nonreactive ensemble members remaining.)

For reaction (R3), we optimized the tunneling path by adjusting the parameter l that appears in the definition of the tunneling direction. Fig. 3 shows the natural logarithm of the non-reactive probability, $\ln(1 - P_r)$, of reaction (R3) using various l values. The simulation with $l = 1$ gives the smallest tunneling probabilities, as seen by the smaller rates of reaction when the energy is lower than barrier. The reaction probabilities of trajectories increase as l is decreased in Fig. 3, and the reaction path with $l = 0.7$ is approximately optimized, at least in a microcanonical ensemble sense.

Reaction rate constants k are plotted as functions of total energy E in Fig. 4 and 5. Although some total energies are greater than the barrier height, the reader should keep in mind that most of the initial energy is not in the reaction coordinate and is not available for surmounting the barrier due to approximate vibrational adiabaticity in the threshold region of a chemical reaction.[31] Thus the reaction rate is dominated by tunneling at these energies. When tunneling is included, the rate constant $k(E)$ decreases smoothly as the energy is lowered until the classical rate is too slow to calculate. The rate constants depend on the l values for reaction (R3), and the optimum l value for the rate constants is approximately $l = 0.7$, which is consistent with Fig. 3. One expects that the tunneling may be underestimated because the tunneling paths are not fully optimized; full optimization is not practical in semi-classical methods, but research into optimization is an interesting subject of further research.

Note that internal coordinates are nonlinear functions of atomic Cartesians, whereas conventional normal-mode coordinates are rectilinear in Cartesians. A major advantage of internal coordinates over rectilinear coordinates is that rectilinear coordinates usually become unphysical for large deviations from equilibrium structures. For example, HCOH has one normal mode for torsional motion, but a large-amplitude motion along this rectilinear normal-mode coordinate not only changes the torsion angle but also changes C–H and O–H bond lengths, which leads to nonphysical tunneling paths and negligible tunneling probabilities. Our method overcomes this problem by using internal coordinates, and we do obtain appreciable tunneling probabilities.

For the HCOH isomerization (R1) when $E = 1.56$ eV, 2.4% of the trajectories react without tunneling; for the HN_2 case when $E = 0.74$ eV, 24% of the trajectories react without tunneling.
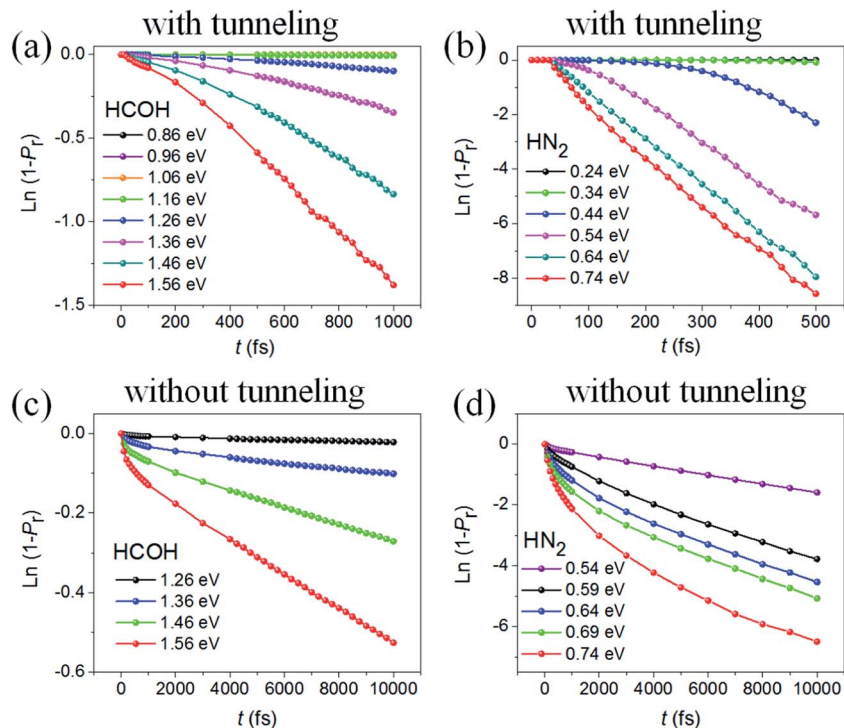
Fig. 2 Natural logarithm of nonreactive probability $\ln(1 - P_r)$ vs. time at various total energies. The HCOH plots are for the cis-HCOH → trans-HCOH reaction, and the HN$_2$ plots are for the HN$_2$ → H + N$_2$ reaction.
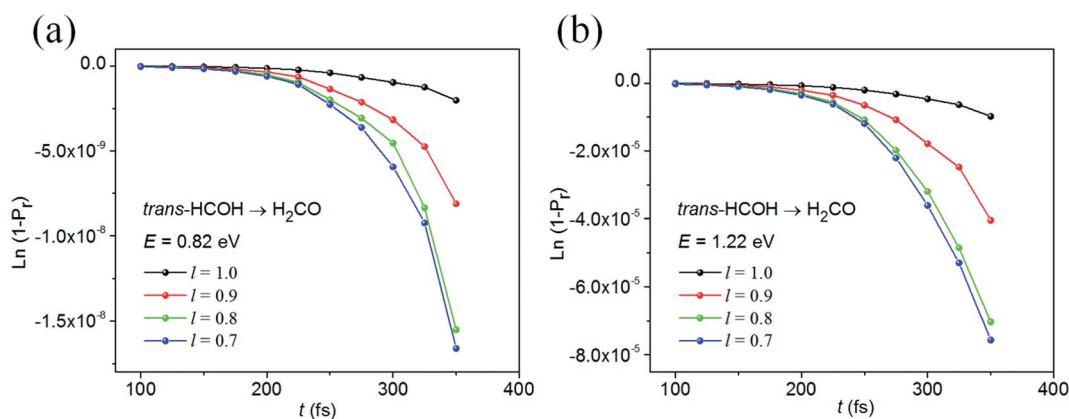

Fig. 3 Natural logarithm of nonreactive probability $\ln(1 - P_r)$ vs. time for the trans-HCOH to H$_2$CO reaction (R3) at total energy $E = 0.82$ eV (a) and $E = 1.22$ eV (b), using various l values.

Here, "react without tunneling" refers to the trajectories that react before any tunneling branching criterion is satisfied; this becomes more important as the energy is raised even in simulations where tunneling is allowed. Note that although only 76% of the reactive events occur by tunneling for the HN$_2$ case with $E = 0.74$ eV, the reaction rate with tunneling at this energy is about two orders of magnitude larger than those calculated without considering tunneling because the rate is determined by the slope of the decay curves in Fig. 2, and the decay of the reactant population is much faster when tunneling is allowed. However, at the lowest energy for which each reaction was studied, all reactions occur by tunneling; for these cases, the

number of tunneling probabilities that falls into each range of order of magnitude is illustrated in Fig. 6 and 7. For (R1) at 0.86 eV, we observed 10 682 tunneling events for 10 000 trajectories (some systems tunnel but do not satisfy the criterion given above for reaction, so we keep integrating, and then they tunnel back); for the cases in Fig. 6(b) and 7, we observe 100 000 tunneling events for 100 000 trajectories in each case. Note that these numbers of tunneling events are those followed according to the army ants algorithm, which means (since η is close to unity) that approximately the same number of potential tunneling events are not followed in the trajectories. In Fig. 6(a), most tunneling events have probabilities between 10^{-16} and
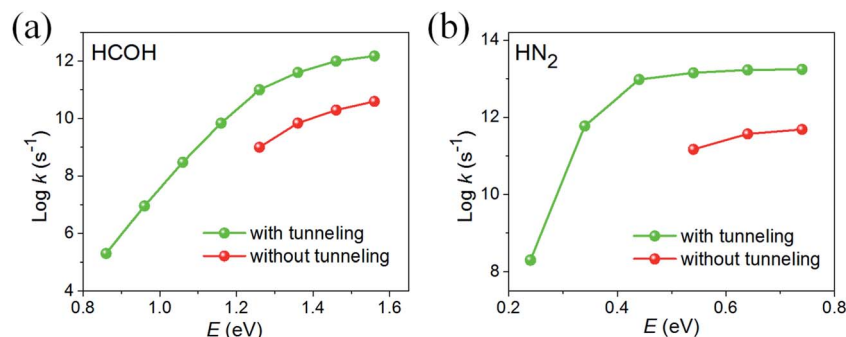
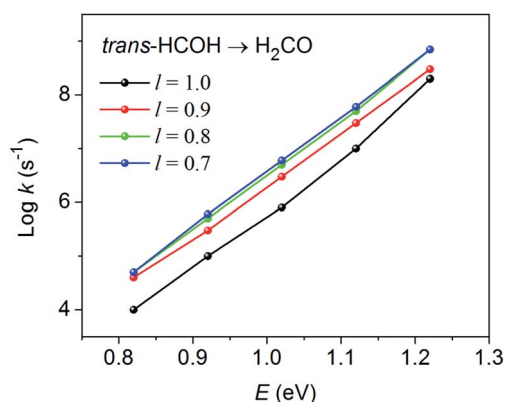Fig. 4   Rate constants $k(E)$ of reactions (R1) (a) and (R2) (b).

Fig. 5   Rate constants $k(E)$ of the *trans*-HCOH to H_2CO reaction (R3) obtained with various l values.

10^{-20}, and tunneling events with probability 10^{-20} or less are accepted 2313 times. In Fig. 6(b), most tunneling events have probabilities between 10^{-5} and 10^{-13}. However the trajectories with very small tunneling probabilities have small weights, and the rate constant for both (R1) and (R2) is dominated by trajectories with tunneling probabilities greater than 10^{-7}.

The tunneling probabilities are spread over a very large range in (R3). Note that the trajectories with $l = 1.0$ have larger number of tunneling events in the peak range (probability from 10^{-14} to 10^{-22}), but the rates are dominated by tunneling events with larger probabilities. The numbers of tunneling events at

0.82 eV total energy with probabilities in the range of 10^{-8} to 10^{-12} are 3072, 3508, 3708, and 3636 for l equal to 1.0, 0.9, 0.8, and 0.7, respectively.

Table 1 lists the computational cost for calculations with tunneling and without tunneling at a given total energy above threshold. Although calculating imaginary action integrals along tunneling paths adds some cost, we see speedup by factors of 3 to 60 due to the faster reaction rates. With the anteater algorithm, most trajectories will not tunnel, so the average time per trajectory will be similar to the runs without tunneling. Since the dominant tunneling probabilities for reactions (R1) and (R2) are about 10^{-4} to 10^{-5}, army ants runs will show a speedup as compared to anteater runs (over and above the speedups in Table 1) of about 4 to 5 orders of magnitude due to not having to run as large a number of trajectories to get good statistics.

Fig. 8 shows that the induction time depends on the value of η used in the tunneling branching, *i.e.*, smaller η values give longer induction times. One can imagine that the induction time would be longer than the longest practical simulation time if η were zero (equivalent to the anteater algorithm) because the probability of following a tunneling path is very low for small η, and it is hard to observe any tunneling events with a reasonable number of trajectories. However, as shown in Fig. 8, after the induction period is over, one obtains similar slopes and hence similar rate constants for the different values of η. Although reaction rate constants converged with respect to the number of trajectories would not depend on η, the reader should be aware
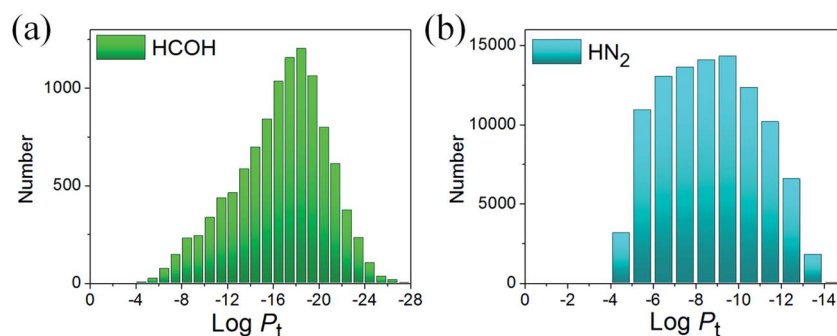

Fig. 6   Number of tunneling probabilities that fall into each range of order of magnitude. (a) 10 000 trajectories of (R1) with total energy 0.86 eV (b) 100 000 trajectories of (R2) with total energy 0.24 eV.
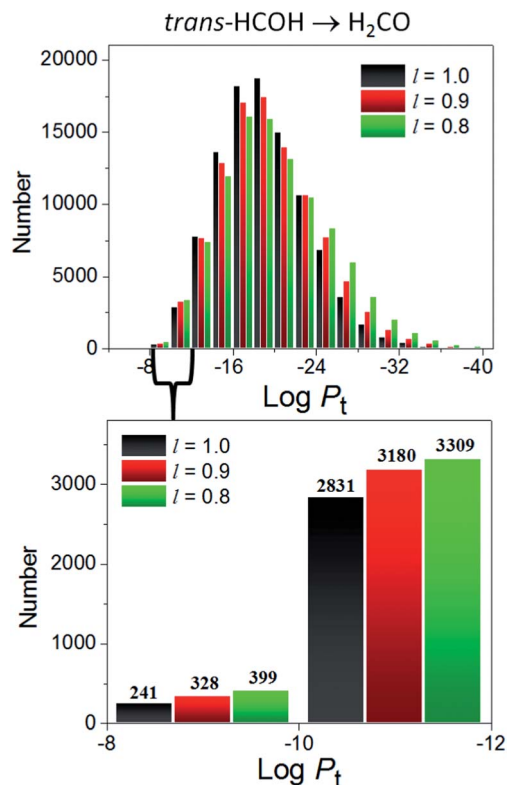
Fig. 7 Number of tunneling probabilities that fall into each range of order of magnitude for the *trans*-HCOH to H_2CO reaction (R3) at total energy $E = 0.82$ eV, obtained by various l values. The logarithms are common logarithms in this figure.

Table 1 Computation times[a] (in hours)

Reaction	With tunneling	Without tunneling
(R1)[b]	0.05	2.92
(R2)[c]	0.03	0.10

[a] Calculations were performed in parallel using 80 processors on an HP Linux cluster, each with two quad-core 2.8 GHz Intel Xeon processors. [b] Total energy is 1.36 eV and 10 000 trajectories are calculated for the timing test. [c] Total energy is 0.64 eV and 100 000 trajectories are calculated for the timing test.

that MD simulations with a finite amount of sampling always depend to some extent on the nature and extent of the sampling leading to some statistical uncertainty,[32–35] as shown by the variation of about 15% in Fig. 8. The variation of the results with η is smaller than the combined uncertainty due to finite statistics, the initialization algorithm, and the induction time.

We have shown previously in the context of variational transition state theory in which all degrees of freedom can be quantized[36–43] that semiclassical tunneling methods can be quantitatively accurate for small molecules and for enzyme kinetics.[13,44–49] Here we combined the same kind of semiclassical tunneling methods with classical molecular dynamics in a practical way; this involves additional approximations because non-tunneling degrees of freedom are not quantized in classical molecular dynamics simulations, an issue that is not solved here
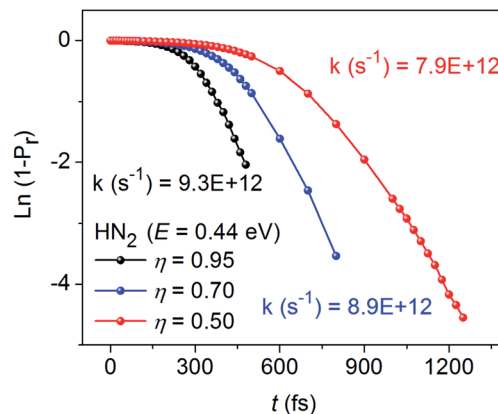

Fig. 8 Natural logarithm of nonreactive probability $\ln(1 − P_r)$ vs. time using various η values for HN_2 dissociation.

but that needs to be addressed in future work. Nevertheless the method as presented eliminates the qualitative error of not including tunneling, and it allows simulations to access product regions that are inaccessible in the absence of tunneling.

Concluding remarks

In this article, we present the army ants tunneling method using internal coordinates to define tunneling paths for classical trajectories, and we demonstrate the method by calculating classical trajectories with tunneling in a single valence coordinate for two example reactions and in a combination of two internal coordinates for one atom-transfer reaction. One of the main goals of the method is to allow one to explore regions of phase space reached only by tunneling, because they may lead to different products or different energy distributions than are populated by non-tunneling processes. The army ants algorithm allows tunneling to be included in classical trajectories very efficiently; the full calculations on an ensemble are less computationally expensive than calculating the reaction rate without tunneling. The army ants tunneling method is designed to be applicable to dynamical processes in arbitrarily large systems, for example, catalysis by enzymes or at heterogeneous interfaces, and it also can be extended to electronically nonadiabatic dynamics. It is reasonably straightforward to add to any classical molecular dynamics program so that one can explore regions of space reached only by tunneling.

Acknowledgements

References

1 L. M. Raff and D. L. Thompson, in *Theory of Chemical Reaction Dynamics*, ed. M. Baer, CRC press, Boca Raton, 1985, pp. 1–123.

2 R. V. Stanton, J. L. Miller and P. A. Kollman, in *Modern Methods for Multidimensional Dynamics Computations in Chemistry*, ed. D. L. Thompson, World Scientific, Singapore, 1998, pp. 355–383.

3 M. Karplus, R. N. Porter and R. D. Sharma, *J. Chem. Phys.*, 1965, **43**, 3259.

4 Y. Guo, D. L. Thompson and T. D. Sewell, *J. Chem. Phys.*, 1996, **104**, 576.

5 D. Bonhommeau and D. G. Truhlar, *J. Chem. Phys.*, 2008, **129**, 014302.

6 J.-P. Ryckaert, G. Ciccotti and H. J. C. Berendsen, *J. Comput. Phys.*, 1977, **23**, 327.

7 E. J. Heller, *J. Chem. Phys.*, 1975, **62**, 1544.

8 D. G. Truhlar and B. C. Garrett, *Annu. Rev. Phys. Chem.*, 1984, **35**, 159.

9 B. C. Garrett, D. G. Truhlar, A. F. Wagner and T. H. Dunning, Jr, *J. Chem. Phys.*, 1983, **78**, 4400.

10 A. Fernandez-Ramos and D. G. Truhlar, *J. Chem. Phys.*, 2001, **114**, 1491.

11 B. C. Garrett and D. G. Truhlar, *J. Chem. Phys.*, 1983, **79**, 4931.

12 R. Meana-Pañeda, D. G. Truhlar and A. Fernández-Ramos, *J. Chem. Theory Comput.*, 2010, **6**, 6.

13 T. C. Allison and D. G. Truhlar, in *Modern Methods for Multidimensional Dynamics Computations in Chemistry*, ed. D. L. Thompson, World Scientific, Singapore, 1998, pp. 618–712.

14 E. J. Heller and R. C. Brown, *J. Chem. Phys.*, 1983, **79**, 3336.

15 N. Makri and W. H. Miller, *J. Chem. Phys.*, 1989, **91**, 4026.

16 J. C. Tully and R. K. Preston, *J. Chem. Phys.*, 1975, **55**, 562.

17 Y. Guo and D. L. Thompson, in *Modern Methods for Multidimensional Dynamics Computations in Chemistry*, ed. D. L. Thompson, World Scientific, Singapore, 1998, pp. 713–737.

18 K. Yagi, T. Taketsugu and K. Hirao, *J. Chem. Phys.*, 2001, **115**, 10647.

19 K. Giese, H. Ushiyama and O. Kühn, *Chem. Phys. Lett.*, 2003, **371**, 681.

20 S. Nangia, A. W. Jasper, T. F. Miller III and D. G. Truhlar, *J. Chem. Phys.*, 2004, **120**, 3586.

21 D. G. Truhlar, R. W. Olson, A. C. Jeannotte II and J. Overend, *J. Am. Chem. Soc.*, 1976, **98**, 2373.

22 G. A. Natanson, B. C. Garrett, T. N. Truong, T. Joseph and D. G. Truhlar, *J. Chem. Phys.*, 1991, **94**, 7875.

23 C. F. Jackels, Z. Gu and D. G. Truhlar, *J. Chem. Phys.*, 1995, **102**, 3188.

24 (*a*) R. A. Marcus and M. E. Coltrin, *J. Chem. Phys.*, 1977, **67**, 2609; (*b*) M. M. Kreevoy, D. Ostović, D. G. Truhlar and B. C. Garrett, *J. Phys. Chem.*, 1986, **90**, 3766; (*c*) T. N. Truong, D. G. Truhlar, J. R. Chelikowsky and M. Y. Chou, *J. Phys. Chem.*, 1990, **94**, 1973; (*d*) B. C. Garrett and D. G. Truhlar, *J. Phys. Chem.*, 1991, **95**, 10374; (*e*) S. E. Wonchoba and D. G. Truhlar, *J. Chem. Phys.*, 1993, **99**, 9637; (*f*) C. Alhambra, J. C. Corchado, M. L. Sanchez, J. Gao and D. G. Truhlar, *J. Am. Chem. Soc.*, 2000, **122**, 8197; (*g*) P. F. Faulder, G. Tresadern, K. K. Chohan, N. S. Scrutton, M. J. Sutcliffe, I. H. Hillier and N. A. Burton, *J. Am. Chem. Soc.*, 2001, **123**, 8604; (*h*) C. S. Tautermann, A. F. Voegele, T. Loerting and K. R. Liedl, *J. Chem. Phys.*, 2002, **116**, 1962; (*i*) Q. Cui and M. Karplus, *J. Am. Chem. Soc.*, 2002, **124**, 3093; (*j*) D. G. Truhlar, J. Gao, M. Garcia-Viloca, C. Alhambra, J. Corchado, M. L. Sanchez and T. D. Poulsen, *Int. J. Quantum Chem.*, 2004, **100**, 1136; (*k*) A. Dybala-Defratyka, P. Paneth, R. Banerjee and D. G. Truhlar, *Proc. Natl. Acad. Sci. U. S. A.*, 2007, **104**, 10774; (*l*) J. Pang, S. Hay, N. S. Scrutton and M. J. Sutcliffe, *J. Am. Chem. Soc.*, 2008, **130**, 7092; (*m*) D. G. Truhlar, in *Isotope Effects in Chemistry and Biology*, ed. A. Kohen and H.-H. Limbach, Marcel Dekker, Inc., New York, 2006, pp. 579–619; (*n*) A. Dybala-Defratyka, P. Paneth and D. G. Truhlar, in *Quantum Tunneling in Enzyme-Catalyzed Reactions*, ed. R. K. Allemann and N. S. Scrutton, RSC Publishing, Cambridge, UK, 2009, p. 36–78; (*o*) J. Zheng and D. G. Truhlar, *Faraday Discuss.*, 2012, **157**, 59.

25 E. B. Wilson, Jr, J. C. Decius and P. C. Cross, *Molecular Vibrations*, McGraw-Hill, New York, 1955, pp. 54–76.

26 P. Pulay, G. Fogarasi, F. Pang and J. E. Boggs, *J. Am. Chem. Soc.*, 1979, **101**, 2550.

27 M. P. Repasky, J. Chandrasekhar and W. L. Jorgensen, *J. Comput. Chem.*, 2002, **23**, 1601.

28 J. Zheng, Z. H. Li, A. W. Jasper, D. A. Bonhommeau, R. Valero, R. Meana-Pañeda and D. G. Truhlar, *ANT program, a modified version based on version 13*, University of Minnesota, Minneapolis, 2013.

29 J. J. P. Stewart, L. J. Fiedler, P. Zhang, J. Zheng, I. Rossi, W.-P. Hu, G. C. Lynch, Y.-P. Liu, Y.-Y. Chuang, J. Pu, J. Li, C. J. Cramer, P. L. Fast and D. G. Truhlar, *MOPAC-mn program, version 5.020*, University of Minnesota, Minneapolis, 2013.

30 H. Koizumi, G. C. Schatz and S. P. Walch, *J. Chem. Phys.*, 1991, **95**, 4130.

31 R. A. Marcus, *J. Chem. Phys.*, 1965, **43**, 1598.

32 D. G. Truhlar and J. T. Muckerman, in *Atom–Molecule Collision Theory: A Guide for the Experimentalist*, ed. R. B. Bernstein, Plenum Press, New York, 1979, p. 505–566.

33 L. S. D. Caves, J. D. Evanseck and M. Karplus, *Protein Sci.*, 1998, **7**, 649.

34 D. Frenkel and B. Smit, *Understanding Molecular Simulation: From Algorithms to Applications*, Academic Press, San Diego, 1996, p. 525.

35 T. Schlick, *Molecular Modeling and Simulation: An Interdisciplinary Guide*, Springer, New York, 2002, p. 368–370.

36 B. C. Garrett and D. G. Truhlar, *J. Chem. Phys.*, 1979, **70**, 1593.

37 D. G. Truhlar and B. C. Garrett, *Acc. Chem. Res.*, 1980, **13**, 440.

38 D. G. Truhlar, A. D. Isaacson, R. T. Skodje and B. C. Garrett, *J. Phys. Chem.*, 1982, **86**, 2252.

39 R. T. Skodje, D. G. Truhlar and B. C. Garrett, *J. Chem. Phys.*, 1982, **77**, 5955.

40 B. C. Garrett and D. G. Truhlar, *J. Chem. Phys.*, 1984, **81**, 309.

41 D. C. Chatfield, R. S. Friedman, D. G. Truhlar, B. C. Garrett and D. W. Schwenke, *J. Am. Chem. Soc.*, 1991, **113**, 486.

42 M. Garcia-Viloca, C. Alhambra, D. G. Truhlar and J. Gao, *J. Chem. Phys.*, 2001, **114**, 9953.

43 A. Fernandez-Ramos, B. A. Ellingson, B. C. Garrett and D. G. Truhlar, in *Reviews in Computational Chemistry*, ed. T. R. Cundari and K. B. Lipkowitz, Wiley-VCH, Hoboken, NJ, 2007, vol. 23, p. 125–232.

44 S. E. Wonchoba and D. G. Truhlar, *J. Chem. Phys.*, 1993, **99**, 9637.

45 J. Pu and D. G. Truhlar, *J. Chem. Phys.*, 2002, **117**, 1479.

46 S. L. Mielke, K. A. Peterson, D. W. Schwenke, B. C. Garrett, D. G. Truhlar, J. V. Michael, M.-C. Su and J. W. Sutherland, *Phys. Rev. Lett.*, 2003, **91**, 63201.

47 D. G. Truhlar, J. Gao, M. Garcia-Viloca, C. Alhambra, J. Corchado, M. L. Sanchez and T. D. Poulsen, *Int. J. Quantum Chem.*, 2004, **100**, 1136.

48 J. Pu, J. Gao and D. G. Truhlar, *Chem. Rev.*, 2006, **106**, 3140.

49 A. Dybala-Defratyka, P. Paneth, R. Banerjee and D. G. Truhlar, *Proc. Natl. Acad. Sci. U. S. A.*, 2007, **104**, 10774.